DOI 10.1007/s11182-018-1495-2

Russian Physics Journal, Vol. 61, No. 6, October, 2018 (Russian Original No. 6, June, 2018)

INFLUENCE OF THE SOLVENT ON THE STRUCTURE AND MORPHOLOGY OF NANOPARTICLES FABRICATED BY LASER ABLATION OF BULK MAGNESIUM TARGETS

V. A. Svetlichnyi, D. A. Goncharov, I. N. Lapin, and A. V. Shabalina UDC 621.373.826, 621.318.1

Ultrafine powders and colloid solutions of nanoparticles are fabricated by nanosecond pulsed laser ablation (a Nd:YAG *laser, 1064 nm, 7 ns, 150 mJ, and 20 Hz) of metallic magnesium targets in water and organic solvents of different polarities (ethyl alcohol, ethyl acetate, and n-hexane). The morphology, dimensional characteristics, composition, and structure of the particles are studied by the methods of transmission electron microscopy, x-ray diffraction, and Fourier-transform infrared spectroscopy depending on the solvent used. For the first time it has been demonstrated that nanostructures of magnesium oxyhydroxide* $Mg_5O(OH)_8$ *are formed during the ablation in water. It is established that in organic solvents, formation of hexagonal and cubic magnesium oxides is possible. Nanoparticles fabricated by the ablation in less thermostable solvents – ethyl acetate and hexane – contain carbonates.*

Keywords: pulsed laser ablation, nanoparticles, crystal structure, magnesium hydroxide, oxyhydroxide, lamella, cubic and hexagonal magnesium oxide, influence of the solvent.

INTRODUCTION

Magnesium is one of the most widespread elements of the Earth crust. It is encountered in the form of different compounds, the most widespread of which are $Mg(OH)_2$ (brucite) and carbonate $MgCO_3$ (magnesite). Magnesium oxide MgO (in the form of mineral periclase) is much less often encountered; it can be fabricated by magnesite decomposition. In the metallic form, magnesium represents a very light (~1.7 g/cm^3) ductile material of silver-white color.

Magnesium compounds play an important role in many practical applications. Thus, magnesium hydroxide is nontoxic, corrosion-resistant, heat-resistant, and environmentally friendly antipyrine subject to endothermic dehydration and vapor suppression during fires. Because of these properties, $Mg(OH)_2$ is widely used as a filler in plastics, rubbers, and other halogen-free polymeric materials [1] functioning as a dye (bleach).

Magnesium is a sufficiently active chemical element (electrochemical potential $\varphi^0 = -2.372$) of the 2nd group belonging to alkali earth metals; it participates in oxidation-reduction reactions in water solutions. Magnesium hydroxide is also used as a neutralizer for treatment of acid sewages and gases [2]. $Mg(OH)_2$ plays an important role in pharmaceutics – it is used as an antacid for treatment of stomach diseases [3] and as a filler in pharmaceutical preparations. Magnesium hydroxide is also used as a precursor to fabricate magnesium oxide. The size and morphology of the final MgO particle depend essentially on the $Mg(OH)_2$ predecessor in the process of topochemical decomposition (in this case, annealing).

Magnesium oxide is a wideband semiconductor (band gap ~7.7 eV) with the refractive index sufficiently large for oxides (n = 1.72 at a wavelength of 1 μm). Because of such optical properties, MgO is widely used as a standard of

National Research Tomsk State University, Tomsk, Russia, e-mail: v_svetlichnyi@bk.ru; dg_va@list.ru; 201kiop@mail.ru; shabalinaav@gmail.com. Translated from Izvestiya Vysshikh Uchebnykh Zavedenii, Fizika, No. 6, pp. 42–48, June, 2018. Original article submitted April 27, 2018.

white color in the wavelength range 0.2–7 μm. In a number of applications, for example in medicine or as antipyrenes or fillers, magnesium oxide is used similar to hydroxide. In food industry it is well known as E530 food additive – emulsifier insoluble in water. It is used for preparation of dry milk and cream, chocolate, and food oils. Magnesium plays an important role in nature being one of the key elements of plants and human bodies.

Of great interest are nanomaterials of different forms and structures based on magnesium compounds. Nanostructures of magnesium compounds are fabricated in different ways. For example, nanohydroxide can be fabricated by the hydrothermal method [4], solvothermal reactions [5–7], sedimentation [8, 9], or pulsed laser ablation (PLA) in a liquid [10, 11]. Nanosized magnesium-based materials demonstrate interesting physicochemical and functional properties. Thus, in [12] it was demonstrated that nanosized magnesium hydroxide demonstrated nonlinear optical properties. The MgO nanocrystals of complex shapes provide high specific surface activity [13] and excellent adsorption properties [14]. Because of spatial anisotropy, the MgO nanostructures also possess specific magnetic properties [15].

Nanosized magnesium oxide is most often fabricated from hydroxide by drying/annealing [14]. However, MgO can be fabricated in one stage, for example, by the laser ablation of metallic magnesium in the liquid – water with corresponding precursors [11, 15]. It should be noted that among different chemical and physical methods of synthesis of nanoparticles (NPs) based on magnesium, the laser ablation in a liquid is a fairly attractive method that allows one to control over the composition and structure of the fabricated nanoparticles, because magnesium belongs to chemically active metals. At the same time, only few works devoted to nanoparticle synthesis by the PLA of magnesium in a liquid have been published by the present time (for example, see [10–12, 15–20]), and the information presented in them is insufficient for establishing laws of directed synthesis of particles with preset compositions and properties.

The present work is aimed at studying the influence of the solvent on the dimensional characteristics, morphology, and structure of nanoparticles fabricated by the nanosecond pulsed laser ablation of metallic magnesium targets in water and in a number of organic solvents without additional precursors to determine conditions of fabrication of magnesium-based ultrafine nanosized structures of different compositions.

EXPERIMENTAL

Fabrication of colloid solutions of nanoparticles

The colloid solutions of NPs were fabricated by the PLA of a metallic magnesium target in a liquid. As a target material, high-purity (99.95%) magnesium (MG95 in accordance with GOST 804-93 and Mg99.95A in accordance with ISO 8287(00)) was used. As liquids, solvents with different boiling temperatures (T_{vap}) and polarities (E_T^N) were used as liquids. Among them were freshly prepared distilled water, rectified ethyl alcohol of "Lux" brand in accordance with GOST 5962-2013 with alcohol content no less than 96.3 volume % without further purification (foreign analog is Ethanol Analytical Specification), ethyl acetate, and chemically pure (>99%) *n*-hexane. Experiments on the PLA were performed on the setup described in [21].

The parallelepiped target of 10 × 25 × 5 mm was fixed in a stainless steel holder and submerged into an open cylindrical reactor (a glass beaker) with 75 mL of liquid. The target was automatically moved in the *X*–*Y* plane orthogonal to the laser beam using two motorized linear translation stages (Standa 8MT175-100). Motion provided uniform exposure of the entire target surface without formation of craters.

Radiation of the fundamental harmonic of a Nd:YAG laser (LS2131M-20, LOTIS TII; 1064 nm, 180 mJ, 7 ns, and 20 Hz) was focused by a short-focus lens with F = 50 mm onto the target surface through the lateral surface of the glass reactor. The liquid layer in front of the target was ~5 mm thick, which minimized the secondary interaction of NPs in the colloid with radiation. The power density that was relatively low for the PLA with nanosecond excitation was determined by thermophysical characteristics of the magnesium target influencing the efficiency and threshold characteristics of the process – relatively low melting and evaporation temperature (650 and 1120°C) and heat (9 and 131 kJ/mol), respectively. All samples were irradiated under identical conditions during 120 min. The mass concentration of nanoparticles fabricated by the PLA was estimated from the loss of the target mass and was in the range 0.5–1 g/L. The freshly prepared dispersions were dried in air at temperatures of 40–50°C. The fabricated ultrafine

powders were additionally mechanically grinded. Depending on the solvent used for the PLA (water, ethanol, ethyl acetate, or *n*-hexane), the samples were marked as Mg_H_2O, Mg_EtOH, Mg_EtAc, and Mg_Hex, respectively.

Method of research

The morphology of the fabricated NPs was studied by the method of transmission electron microscopy (TEM) using a CM 12 Philips microscope (the Netherlands) with accelerating voltage of 120 kV. To perform microscopic studies, the examined powders were re-dispersed in ethyl alcohol, ultrasonicated, and deposited on a copper grid for microscopy with an amorphous carbon film on the surface. Then the grid was dried at room temperature.

The crystal structure of the powders was studied by the x-ray diffraction method on an XRD 6000 Shimadzu (Japan) using CuK_α radiation with a wavelength of 1.54056 Å, scanning angles in the range 10–70°, and scanning step of 0.02°. The phase composition was identified using the PDF-4 database. The percentage of crystal phases in the samples was estimated using the *PowderCell 2.4* program complex.

The specific surface area and the pore size distribution were determined from the data obtained using a TriStar II 3020 Micromeritics gas adsorption analyzer of specific surface and porosity. Before analysis, the samples were degassed in vacuum (10^{-2} Torr) at 200°C for 2 h. Nitrogen was used as a gas during measurements.

The absorption spectra of powders in the IR range were studied by the method of attenuated total internal reflection (ATIR). Measurements were performed using a Nicolet 6700 FT-IR spectrometer (Thermo Fisher Scientific, the USA). The reflection spectra were converted into the absorption spectra using the Kubelka–Munk transformation.

RESULTS AND DISCUSSION

The method of transmission electronic microscopy was used to study the microstructure of the NPs fabricated from the colloid solutions. The TEM image in Fig. 1*a* illustrates the morphology of nanostructures fabricated by the PLA of magnesium in water. It can be seen that the sample is represented by lamellar (leafy, scaly) structures, the so-called lamellas [23]. These are two-dimensional structures with length and width from several nanometers to a micron. Because of small thickness (up to 5–10 nm), the lamellas can undergo mechanical deformations, namely, can be folded, bent, or twisted. When dried, these lamellas form sufficiently densely packed structures with specific surface area of only 8 m^2/g (Table 1). The morphology of fabricated particles correlated with the data obtained by other authors (for example, see [11, 16]) using the nanosecond PLA of magnesium in water without precursors. At the same time, depending on the parameters of the experiment, in particular, on the laser radiation parameters (wavelength, pulse length, and pulse power density), the sizes and morphology of the nanostructures can differ [10, 12] demonstrating sufficiently great diversity.

The nanoparticles fabricated by the PLA in organic solvents (Fig. 1*b*-*g*) have shapes close to spherical ones. Moreover, larger particles are in minority and are shaped as hollow spheres (the density of the substance in the centre of the structure is less than on the periphery). Large structures are surrounded by the more homogeneous small (≥5 nm) particles assembled in chained agglomerates. The smallest sizes (predominantly up to 10 nm) have the nanoparticles fabricated by the PLA from magnesium in ethanol. These data are confirmed by measurements of the specific surface area of nanopowders: the greatest S_{BET} corresponds to the smallest nanoparticles fabricated in ethanol – 380 m^2/g. For particles fabricated by the PLA in ethyl acetate and *n*-hexane, the specific surface area was 221 and 133 m^2/g, respectively.

Results of investigation of the crystal structure of nanoparticles obtained in the present work by the XRD method are shown in Fig. 2*a*. According to a few data presented in the literature, during the PLA of magnesium in water the hexagonal phase of hydroxide [10–12] is formed. Surfactant additives of dodecyl sulfate type [10, 16] or less polar solvents lead also to the formation of oxide with insignificant amount of remaining metal phase [11, 15, 20]. At the same time, detailed analysis of our results and the literature data mentioned above demonstrated that in water solutions, oxyhydroxide $Mg_5O(OH)_8$ from the series $Mg_{x+y}O_x(OH)_{2y}$ is predominantly formed rather than classical hexagonal magnesium hydroxide with the *P*-3*m*1 space symmetry group (PDF Card No. 00-007-0239). In our case, $Mg_5O(OH)_8$ is

TABLE 1. Parameters of the Reaction Medium and Properties of Nanopowders Fabricated by the PLA of Magnesium

Solvent	T_{vap}, °C	E_t^N	S_{BET}, m^2/g	Colloid stability	Crystal structure	Morphology
Water	100	1.000	9	+	$Mg_5O(OH)_8$ hexagonal $Mg(OH)_2$ hexagonal MgO hexagonal/cubic	Lamellar
Ethanol	78.3	0.654	380	+	MgO hexagonal/cubic Mg (metal) hexagonal	Spheroidal, hollow
Ethyl acetate	77.1	0.228	221	–	MgO hexagonal/cubic Mg (metal) hexagonal Mg (carbonate/hydrocarbonate)	Spheroidal, hollow
n-hexane	68.7	0.009	133	–	MgO hexagonal/cubic Mg (metal) hexagonal Mg (carbonate/hydrocarbonate)	Spheroidal, hollow

formed also belonging to the *P*-3*m*1 symmetry group (PDF Card No. 00-014-08452). Unlike hydroxide, oxyhydroxide has the XED pattern with a greater number of peaks better corresponding to the experimentally observed XRD pattern (curve *1* in Fig. 2), especially at small angles $2\theta = 10–25°$.

The formation of lamellar hydroxide by the high-energy pulsed laser ablation and the subsequent processes of dehydroxylation play an important role in understanding of the mechanism of highly reactive formation of oxide nanocrystals. Initial lamellas can form a series of solid solutions of intermediate lamellar oxyhydroxide products on the way to the oxide formation. In addition, of fundamental and practical interest are intermediate oxyhydroxide materials formed in the process of dehydroxylation [23].

In addition to above-described oxyhydroxide $Mg_5O(OH)_8$, an insignificant amount of conventional hydroxide was presented in the Mg_H_2O sample, and oxide peaks were also observed. However, it seems impossible to interpret precisely the crystal structure of the oxide – cubic or hexagonal – because of the low intensity and considerable broadening and overlapping of peaks for crystal lattices of different types.

Similar to [15], the PLA in ethanol after drying caused the formation of magnesium oxide mainly with a small amount of impurity of metallic magnesium (PDF Card No. 01-079-6692). However, unlike [15] where only peaks of cubic MgO were observed and particles were shaped as nanocubes, in our case the XRD pattern showed the presence of a mixture containing cubic magnesium oxide with *Fm*-3*m* space group (PDF Card No. 04-005-4394) and hexagonal magnesium oxide with *P*63/*mmc* space group of symmetry (PDF Card No. 01-080-4184).

The PLA in ethyl acetate and hexane caused decomposition of the solvent leading to the formation on the surface of particles of carbon-containing structures – carbonates and hydrocarbonates. These structures revealed themselves through low-intensive peaks in the corresponding XRD patterns (curves *3* and *4* in Fig. 2*a*). Their presence also resulted in dark grey color of the powders. Hexagonal magnesium and magnesium oxide are the main crystal phases of particles for the Mg_EtAc and Mg_Hex samples. This correlates with the results obtained in [11, 20] by the PLA of magnesium in acetone and mixtures of ethanol and hexane [15]. From the data presented here it is impossible to determine precisely the hydroxide syngony (hexagonal/cubic or their mixture) because of the considerable peak broadening and insufficient peak intensity.

In the FTIR spectra of the fabricated powders (Fig. 2*b*), three main ranges can be identified: 1) 2500–4000 cm^{-1} where vibrations of different types associated with OH groups are presented, 2) 1200–1800 cm^{-1} associated with the presence of CO groups and partially OH groups, 3) shorter than 400–1000 cm^{-1} where vibrations of Mg–O are manifested.

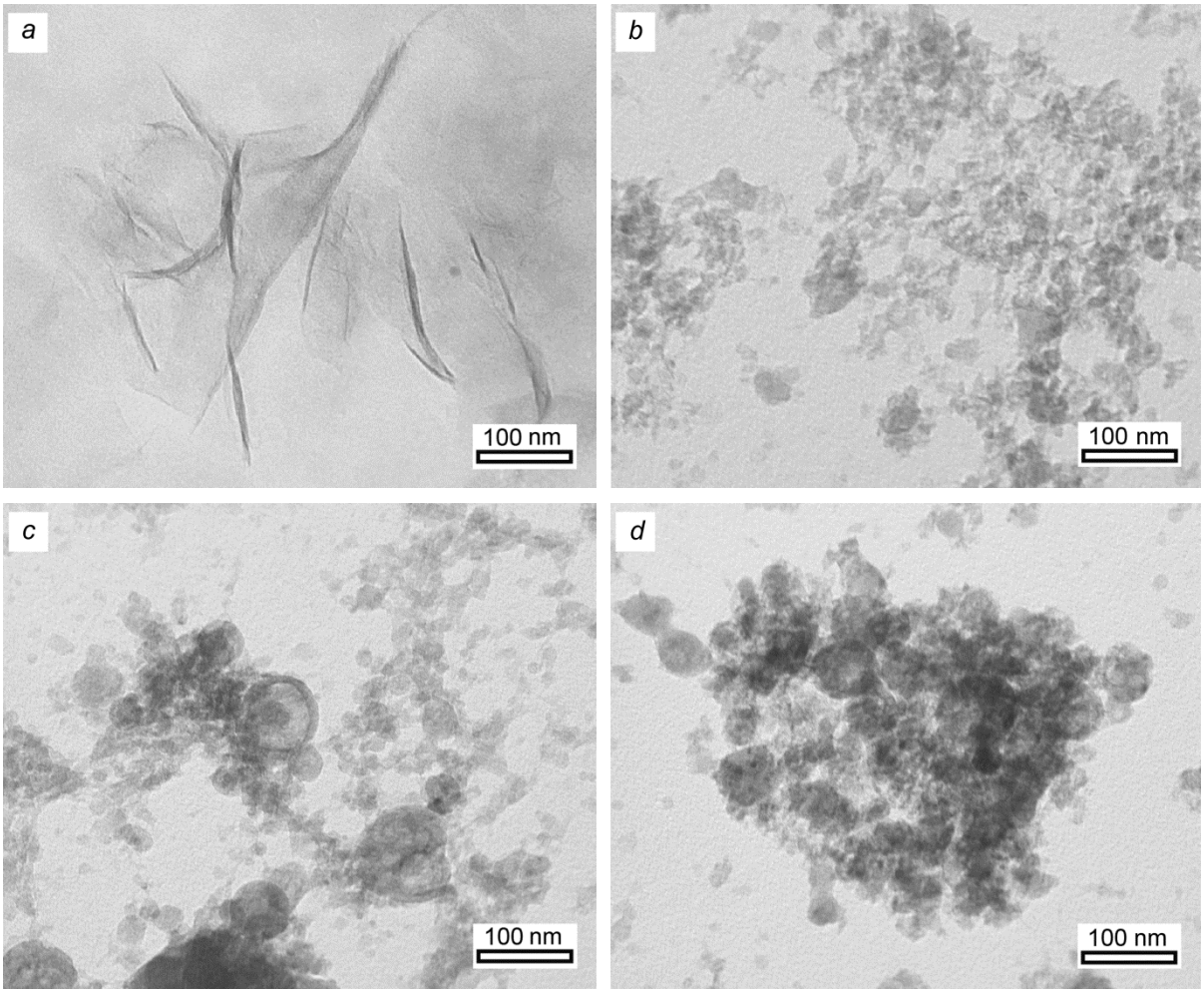

Fig. 1. TEM images of NPs fabricated by the PLA of magnesium in water (*a*), ethanol (*b*), ethyl acetate (*c*), and hexane (*d*).

It should be noted that the FTIR spectra do not allow one to interpret unambiguously the structure of the fabricated particles; however, they supplement well and correlate with the results of XRD analysis. Thus, the intensive narrow peak at 3700 cm^{-1} is conventionally assigned to A_{2u} (OH) vibration of magnesium hydroxide Mg $(OH)_2$ [24]. The wide band in the range 2500–4000 cm^{-1} for all examined powders is attributed to vibrations of OH groups of adsorbed water characteristic for magnesium oxides and hydroxides. The absorption in the region of 1200–1800 cm^{-1} for the samples fabricated by the PLA in organic solvents was attributed to the remaining molecules of the corresponding solvents adsorbed on the particle surface and to carbonates formed by decomposition of solvents upon exposure to high-energy laser radiation. For the sample fabricated by the PLA of magnesium in water, the absorption in this region was associated with adsorbed CO_2 or organic matter as a result of drying of the initial dispersion in air. The wide band with the maximum in the region of ~550 nm refers to stretching vibrations of Mg–O [25], and in agreement with the XRD data, this band is characteristic both for oxide and hydroxide. The narrow absorption peak in the region of 860 cm^{-1} was better expressed for particles fabricated by the PLA in alcohol and ethyl acetate where the content of the oxide according to the XRD data is maximal. According to the literature, this band corresponds to combined vibrations – stretching ν(Mg–O) + deformation δ(O–C=O) [20].

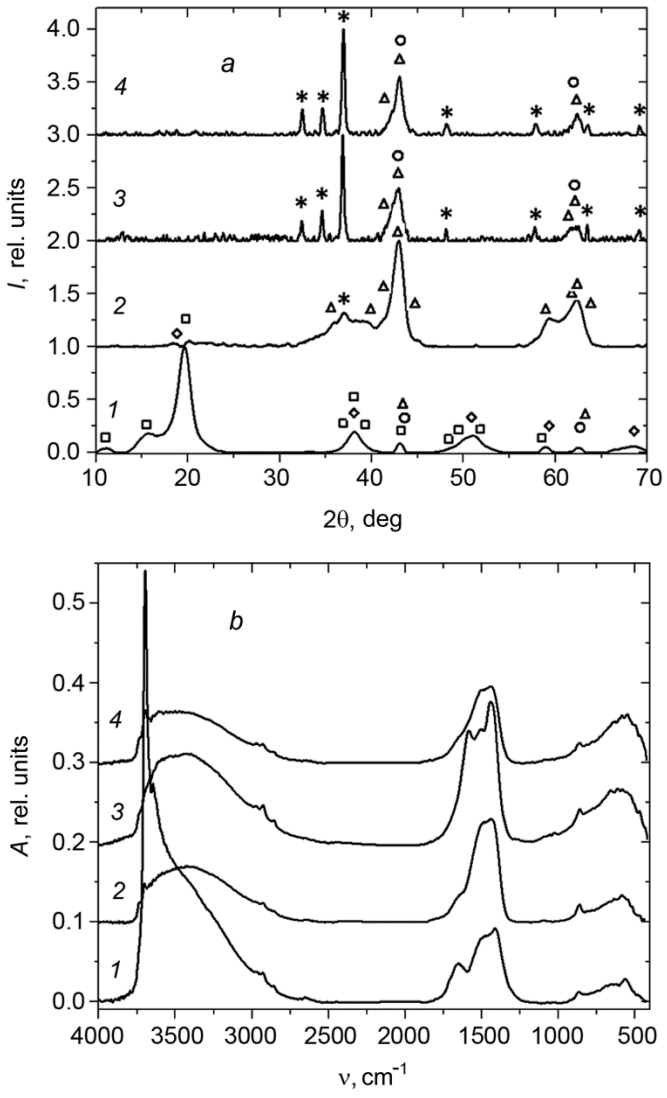

Fig. 2. XRD patterns (*a*) and FTIR spectra (*b*) of the examined Mg_H_2O (curve *1*), Mg_EtOH (curve *2*), Mg_EtAc (curve *3*), and Mg_Hex powders (curve *4*). Symbols mark positions of peaks for hexagonal metal Mg (*), hydroxide $Mg(OH)_2$ (◇), oxyhydroxide $Mg_5O(OH)_8$ (□), MgO (△), and cubic MgO (○).

CONCLUSIONS

Our investigations have demonstrated that the pulsed laser ablation of targets from chemically active metals is an effective method that allows one to control over the final structure of the fabricated nanoparticles. For the magnesium target in different solvents, it is possible to fabricate nanoparticles from magnesium hydroxide to its oxide together with metal Mg without additional precursors. The analysis of the XRD patterns of the fabricated nanostructures demonstrated that during the PLA in water, not simply lamellar magnesium hydroxide is fabricated, as pointed out by other authors, but also more complex structures of oxyhydroxide $Mg_5O(OH)_8$ are formed. This allows one to investigate the processes of lamellar origin and growth, and opens the possibility of fabrication of a series of new $Mg_{x+y}O_x(OH)_{2y}$ materials. Since the properties and structure of magnesium oxides are in many respects determined by the

characteristics of the initial hydroxides, such materials can be not only of independent interest, but also can model intermediate products in the study of reactions of magnesium oxide formation. The directed formation of magnesium oxide with hexagonal or cubic structure can be one of these important problems.

The results presented here were obtained within the framework of execution of the State Assignment of the Ministry of Education and Science of the Russian Federation (Project No. 9604.2017/8.9).

REFERENCES

1. M. Sain, S. H. Park, F. Suhara, and S. Law, Polym. Degrad. Stab., **83**, 363–367 (2004).
2. J. L. Booster, A. V. Sandwijk, and M. A. Reuter, Miner. Eng., **16**, 273–281 (2003).
3. J. Kang and P. Schwendeman, Biomaterials, **23**, 239–245 (2002).
4. C. Henrist, J. P. Mathieu, C. Vogels, *et al*., J. Cryst. Growth, **249**, 321–330 (2003).
5. Y. D. Li, M. Sui, Y. Ding, *et al*., Adv. Mater., **12**, 818–821 (2000).
6. H. Chen, C. Xu, Y. Liu, and G. Zhao, Electron. Mater. Lett., **8**, 529–533 (2012).
7. W. L. Fan, S. X. Sun, L. P. You, *et al*., J. Mater. Chem., **13**, 3062–3065 (2003).
8. B. Li, H. Cao, and G. Yin, J. Mater. Chem., **21**, 13765–13768 (2011).
9. J. P. Lv, L. Z. Qiu, and B. J. Qu, J. Cryst. Growth, **267**, 676–684 (2004).
10. C. Liang, T. Sasaki, Y. Shimizu, and N. Koshizaki, Chem. Phys. Lett., **389**, 58–63 (2004).
11. T. X. Phuoc, B. H. Howard, D. V. Martello, *et al*., Opt. Laser. Eng., **46**, 829–834 (2008).
12. F. Abrinaei, J. Opt. Soc. Am. B, **33**, No. 5, 864–869 (2016).
13. K. J. Klabunde, J. V. Stark, O. Koper, *et al*., J. Phys. Chem., **100**, No. 30, 12142–12153 (1996).
14. R. Richards, W. F. Li, S. Decker, *et al*., J. Am. Chem. Soc., **122**, No. 20, 4921–4925 (2000).
15. K. Y. Niu, J. Yang, S. A. Kulinich, *et al*., J. Am. Chem. Soc., **132**, No. 28, 9814–9819 (2010).
16. Z. Yan, R. Bao, C. M. Busta, and D. B. Chrisey, Nanotechnology, **22**, Art. No. 265610, 1–8 (2011).
17. F. Abrinaei, M. J. Torkamany, M. R. Hantezadeh, and J. Sabbaghzadeh, Sci. Adv. Mater., **4**, No. 3/4, 501–506 (2012).
18. A. Schwenke, P. Wagener, S. Nolte, and S. Barcikowski, Appl. Phys. A, **104**, 77–82 (2011).
19. K. S. Khashan and F. Mahdi, Surf. Rev. Lett., **24**, No. 7, Art. No. 1750101, 1–7 (2017).
20. F. Abrinaei, J. Eur. Opt. Soc.-Rapid Publ., **13**, No. 15, 1–10 (2017).
21. V. A. Svetlichnyi and I. N. Lapin, Russ. Phys. J., **56**, No. 5, 581–587 (2013).
22. V. A. Svetlichnyi and I. N. Lapin, Russ. Phys. J., **57**, No. 12, 1789–1792 (2014).
23. M. J. McKelvy, R. Sharma, A. V. G. Chizgridya, and R. W. Carpenter, Chem. Mater., **13**, No. 3, 921–926 (2001).
24. L.-X. Li, D. Xu, X.-Q. Li, *et al*., New J. Chem., **38**, 5445–5452 (2014).
25. S. Xie, X. Han, Q. Kuang, *et al*., J. Mater. Chem., **21**, 7263–7268 (2011).